arXiv:1005.5476v1 [astro-ph.CO] 29 May 2010

LETTER TO THE EDITOR

Radial distribution of gas and dust in spiral galaxies[*]

The case of M 99 (NGC 4254) and M 100 (NGC 4321)

M. Pohlen[1], L. Cortese[1], M. W. L. Smith[1], S. A. Eales[1], A. Boselli[3], G. J. Bendo[2], H. L. Gomez[1], A. Papageorgiou[1], R. Auld[1], M. Baes[4], J. J. Bock[5], M. Bradford[5], V. Buat[3], N. Castro-Rodriguez[6], P. Chanial[7], S. Charlot[8], L. Ciesla[3], D. L. Clements[2], A. Cooray[9], D. Cormier[7], E. Dwek[10], S. A. Eales[1], D. Elbaz[7], M. Galametz[7], F. Galliano[7], W. K. Gear[1], J. Glenn[11], M. Griffin[1], S. Hony[7], K. G. Isaak[1,12], L. R. Levenson[5], N. Lu[5], S. Madden[7], B. O'Halloran[2], K. Okumura[7], S. Oliver[13], M. J. Page[14], P. Panuzzo[7], T. J. Parkin[15], I. Perez-Fournon[6], N. Rangwala[11], E. E. Rigby[16], H. Roussel[8], A. Rykala[1], N. Sacchi[17], M. Sauvage[7], B. Schulz[18], M. R. P. Schirm[15], M. W. L. Smith[1], L. Spinoglio[17], J. A. Stevens[19], S. Srinivasan[8], M. Symeonidis[14], M. Trichas[2], M. Vaccari[20], L. Vigroux[8], C. D. Wilson[15], H. Wozniak[21], G. S. Wright[22], W. W. Zeilinger[23]

(Affiliations can be found after the references)

ABSTRACT

By combining *Herschel*-SPIRE data with archival *Spitzer*, H I, and CO maps, we investigate the spatial distribution of gas and dust in the two famous grand-design spirals M 99 and M 100 in the Virgo cluster. Thanks to the unique resolution and sensitivity of the *Herschel*-SPIRE photometer, we are for the first time able to measure the distribution and extent of cool, submillimetre (submm)-emitting dust inside and beyond the optical radius. We compare this with the radial variation in both the gas mass and the metallicity. Although we adopt a model-independent, phenomenological approach, our analysis provides important insights. We find the dust extending to at least the optical radius of the galaxy and showing breaks in its radial profiles at similar positions as the stellar distribution. The colour indices $f350/f500$ and $f250/f350$ decrease radially consistent with the temperature decreasing with radius. We also find evidence of an increasing gas to dust ratio with radius in the outer regions of both galaxies.

Key words. Galaxies: evolution – Galaxies: structure – Galaxies: individual: M 99, M 100 – Infrared: galaxies – ISM: dust – Submillimetre: galaxies

1. Introduction

The study of the gas and dust distribution in galaxies is essential to understanding their formation and evolution. The rate at which gas is accreted and converted into stars regulates not only the star formation history of galaxies but also their chemical evolution. Dust is supposed to play a key role in this process. Dust grains are the main coolant in star-forming galaxies, shielding the gas from the UV radiation and representing the site at which H I is converted into H_2, and then collapses into stars (see e.g., reviews by Calzetti, 2001; Draine, 2003).

To understand the dust, we need to map the cold component, which does not dominate the energy but dominates the mass. However, using previously existing facilities, our knowledge of the interplay between gas and dust and their radial distribution have remained highly uncertain, being based only on $\lambda < 160\mu m$ space observations (e.g. Muñoz-Mateos et al., 2009a; Bendo et al., 2010a), and challenging ground-based submm observations that were of optimal quality only at significantly longer wavelength. For many galaxies, only integrated quantities have been derived because of the poor resolution of previous satellites. Resolved submm studies from the ground remain

limited to the very nearby universe and large surveys of more distant galaxies are unfeasible.

The SPIRE instrument (Griffin et al., 2010) on-board *Herschel* (Pilbratt et al., 2010) now bridges this gap observing in the range of $250\mu m$-$500\mu m$. With the benefit of the stable conditions of a space observatory, it is much more sensitive to the cold component and provides excellent maps at high resolution, so is ideal for large surveys of many galaxies. With *Herschel*, we are now able to tackle the problem of the interplay between gas and dust, and combined with the number of recent high resolution surveys tracing the gas mass of local galaxies (e.g. Chung et al., 2009; Kuno et al., 2007), we can study the distribution of gas, metals, and dust on a kpc scale for hundreds of galaxies.

Here, we discuss first results for two famous grand-design spirals M 99 and M 100 (see Fig. 1) in the Virgo cluster. We explore the distribution of the cool dust traced with *Herschel* by inspecting their radial profiles from mid-infrared to submm wavelengths. We then attempt to correlate this with the observed gas and metallicity distributions and search for temperature variations. We use the *Herschel*-SPIRE maps taken during *Herschel*'s Science Demonstration Phase. The two galaxies are part of the *Herschel* Reference Survey (Boselli et al., 2010a). This guaranteed time key project will provide maps for a statistically-complete sample of 323 nearby galaxies in all three SPIRE bands. In the RC3 (de Vaucouleurs et al., 1991), the clas-

---

[*] Herschel is an ESA space observatory with science instruments provided by European-led Principal Investigator consortia and with important participation from NASA
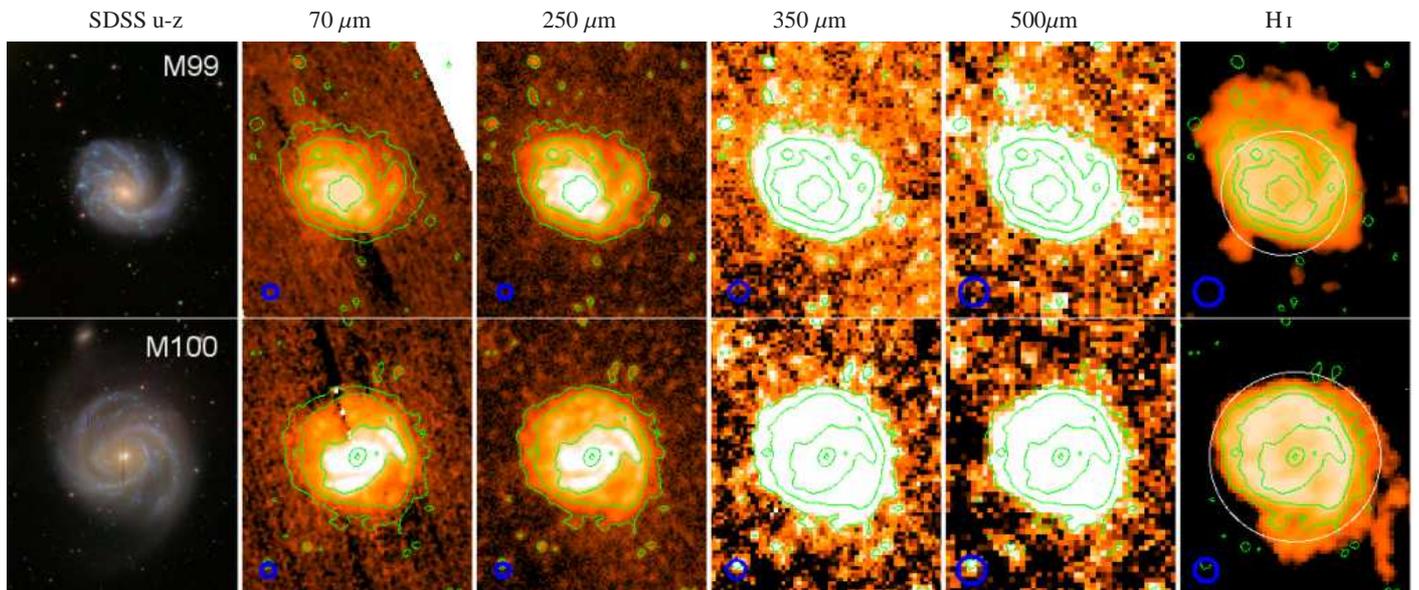
Fig. 1. The matched SDSS, MIPS 70 μm, SPIRE 250, 350, 500 μm, and H I -maps of M 99 *(upper row)* and M 100 *(lower row)*. The *green contours* are SPIRE 250 at levels about 0.03($\approx 5\sigma$), 0.10, 0.34, 1.15, 3.9 Jy beam^{-1}. The 350 and 500 μm are displayed at a high contrast to show the extent of the dust emission and the scan-artefact free smooth background dominated only by confusion noise. The *white circle* on the H I -maps marks the optical radius defined by $D25$. The *blue circles* on each map indicate the FWHM. Note, the SDSS jpg is scaled but not WCS matched.

sification and optical radius $R25$ of M 99 and M 100 is given as SA(s)c, 2.69′($\approx$ 12.9kpc), and SAB(s)bc, 3.71′($\approx$ 17.8kpc), respectively. We assume a distance for the Virgo Cluster of 16.5 Mpc (Mei et al., 2007).

2. Data

2.1. Herschel-SPIRE

The SPIRE photometer (Griffin et al., 2008, 2010) data were processed up to Level-1 (i.e., to the level where the pointed photometer time-lines were derived) with a customised pipeline script adapted from the official pipeline (*POF5_pipeline.py*, dated 27 Nov 2009) provided by the SPIRE Instrument Control Centre (ICC)[1]. This Jython script was run in the *Herschel* Interactive Processing Environment (HIPE Ott, 2010) coming with continuous integration build number 3.0.327, which is the current developer's branch of the data reduction software. However, in terms of the SPIRE scan-map pipeline up to Level-1, this is in principle identical to the *Herschel* Common Science System/Standard Product Generation v2.1, even down to the calibration files[2] associated with the individual pipeline modules. This version of the pipeline is used at ESA to produce the standard products that will be available from the *Herschel* Science Archive once they become public.

Currently, the Level-1 photometer time-lines still requires a residual baseline subtraction to be made. However, instead of subtracting the median of the time-line for each bolometer per scanleg (the default), we subtracted the median of the time-lines for each bolometer over the whole observation. This circumvents shadow artefacts caused in cases where the signal time-lines in

individual scanlegs are dominated by structured emission e.g. a large, extended galaxy or a strong cirrus component.

This baseline-subtracted Level-1 data were then fed through an iterative de-striper, which minimises the difference between the signal in individual detector time-lines and the final map (see Bendo et al., 2010b, for a longer description). At the end of this process, the signal time-lines were then mapped into a final image using the Naive Mapper available in HIPE.

For M 99, the de-striping approach left some residual large-scale gradients. In this case, we resorted back to an initial baseline subtraction on a scan by scan basis. However, instead of a median, we used a robust linear fit with outlier rejection to the first and last fifty sample points, thus avoiding the galaxies in the centre of the time-lines.

According to the ICC, the uncertainty in the flux calibration is of the order of 15% (Swinyard et al., 2010) and is currently based on a preliminary calibration. However, the ICC has released some interim small correction factors to improve this calibration. All flux values derived using the current standard calibration file for the flux conversion, are multiplied by 1.02, 1.05, and 0.94, for the 250μm, 350μm, and 500μm, respectively.[3] The full widths at half maximum (FWHM) of the SPIRE beams are 18.1″, 25.2″, and 36.9″, the pixel sizes are 6″, 10″, and 14″ at 250, 350, and 500 μm, respectively.

For both, M 99 and M 100, we observed a 12′×12′ field doing three repetitions of a cross-linked scan-map at nominal detector settings and nominal scan speed (30″/sec). The M 100 observation was carried out twice. Both were treated independently here and used to verify the consistency of our results.

2.2. MIPS, CO, and HI

The 24, 70, and 160 μm images were part of the SINGS survey (Kennicutt et al., 2003) and were processed using the MIPS Data Analysis Tools (Gordon et al., 2005) along with techniques

---

[1] See 'The SPIRE Analogue Signal Chain and Photometer Detector Data Processing Pipeline' (Griffin, 2009) for a more detailed description of the pipeline and a list of the individual modules.

[2] Aprt from the BsmPos file, for which we use an updated version that should improve the absolute astrometry.

[3] See http://herschel.esac.esa.int/SDP_wkshops/presentations/IR/3_Griffin_SPIRE_SDP
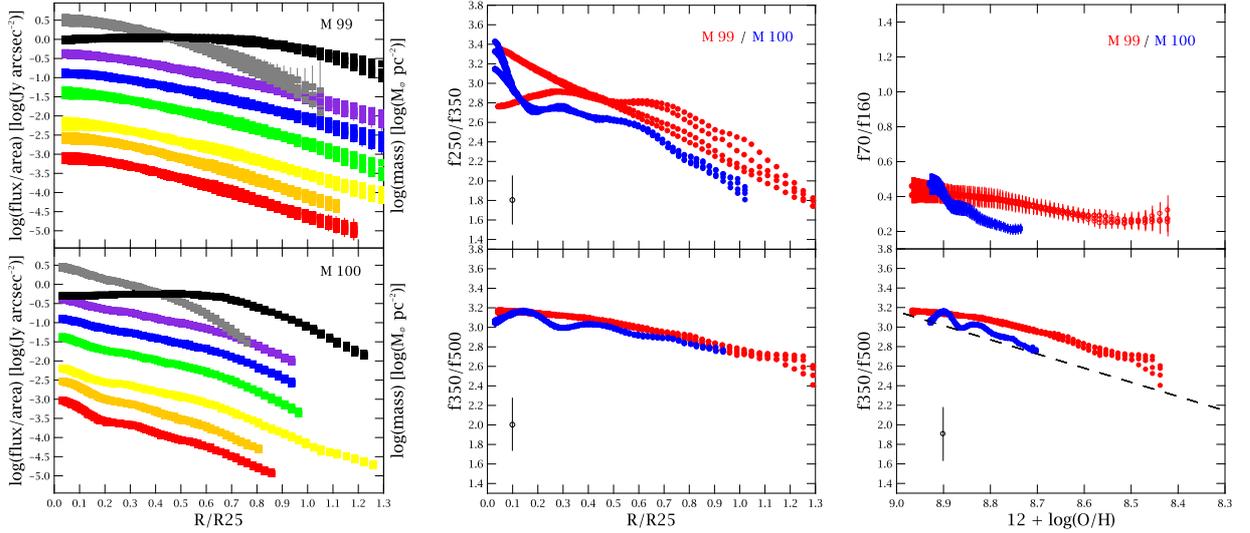
Fig. 2. *Left:* Radial surface brightness profiles for M 99 *(top)* and M 100 *(bottom)* obtained from the smoothed and matched maps (see text). The profiles are from the bottom up: MIPS 24, 70, 160 μm, SPIRE 250, 350, 500 μm (all in [log(Jy/arcsec^2)]), H I *(black)* and H$_2$ [5] *(gray*, both in [log(M$_\odot$/pc^2)]) adding 0.5, 0, 0, 1, 2, 3, -1, -1, respectively, to separate them in the plot and the radial axis is in units of $R25$. In all cases, we plot four different radial profiles per galaxy to show the influence of the fixed ellipse fitting (see Sect. 2.3). *Middle:* SPIRE colours $f350/f500$ and $f250/f350$ with radius for M 99 *(red)* and M 100 *(blue)*. *Right:* $f350/f500$ and $f70/f160$ versus the metallicity again for M 99 in *red* and M 100 in *blue*. Since the uncertainty in the SPIRE flux is still rather large, we only provide an indication of the error in the SPIRE colours with a *black open circle* in the lower left corner of the appropriate panels (see Sect. 2.3). The *dashed black line* in the lower right panel is a fit to the integrated properties of a larger sample of galaxies with a variety of morphologies (Boselli et al., 2010b).

described by Bendo et al. (2010a) and Clements et al. (2010, in preparation). The FWHM of the MIPS beams are about 6″, 18″, and 38″, the pixel sizes are 1.5″, 4.5″, and 9″ per pixel at 24, 70, and 160 μm, respectively. The CO(J=1-0) maps, used as the tracer of the molecular hydrogen dominating the molecular mass, are taken from the Nobeyama CO Atlas of Nearby Spiral Galaxies (Kuno et al., 2007). The FWHM is 15″ and the pixels are 1″ per pixel. For the H I, we used the zeroth moment maps from the VIVA survey (VLA Imaging of Virgo Spirals in Atomic Gas; Chung et al., 2009). The FWHM and pixel sizes are ≈ 37″ and 5″ per pixel for M 99 and ≈ 30″ and 10″ per pixel for M 100.

2.3. Analysis

The SPIRE maps were first converted into Jy per pixel assuming a Gaussian beam (of the above quoted sizes). For the H I, we used the elliptical beam sizes given in Chung et al. (2009). In all maps, we masked strong sources and artefacts. However, in the case of the SPIRE maps, being confusion limited, all faint sources are unmasked and part of the background. The residual background on each map was subsequently determined using IRAF's[4] ELLIPSE task as described in Pohlen & Trujillo (2006). The background-subtracted maps of all wavelengths were thereafter smoothed to the MIPS 160μm resolution of ≈ 40″ using custom convolution kernels derived as described in Bendo et al. (2010a) and then matched to the SPIRE 500μm pixel size of 14″.

The SPIRE 250μm map was chosen to derive the final set of ellipse-fitting parameters (i.e., ellipticity, position angle, and centre). To ensure that our results are independent of the particular ellipse geometry selected, we applied four different fixed ellipse fits to each map. For example, M 99 being a one-armed

spiral, is slightly asymmetric (cf. Fig. 1) so we selected one set of ellipse parameters derived in the outer parts and one in the inner parts, which each have slightly different centres. The final radial profiles, obtained using a combined mask on the smoothed and matched maps, are shown in Fig. 2 out to where we can trace signal on the map. The error bar in each measured point is a combination in quadrature of the uncertainty in the overall absolute calibration (currently for SPIRE the dominating source), the error in the ellipse intensity from the ELLIPSE task, the uncertainty in the estimate of the background, and an additional uncertainty calculated by comparing the results from different versions of the pipeline. This last, very conservative uncertainty, is responsible for the currently rather large error bars in the measured flux ratios in Fig. 2.

3. Results

We detect dust emission traced by all three SPIRE bands out to at least the optical radius defined by $R25$ for both galaxies (see Fig. 1 for ≈ 3 − 5σ detections in the nominal maps, and Fig. 2 for the deeper, radially averaged profiles from the smoothed maps). Compared to H I, the dust can be found almost out to the H I-edge of the regular disk for M 100. This is not entirely surprising, since M 100 is an intermediate H I-deficient (Haynes & Giovanelli, 1984; Cayatte et al., 1994) galaxy (H I-def= 0.35) and thus its outer H I-disk has probably been already stripped by the interaction with the cluster environment (Boselli & Gavazzi, 2006). A similar extension of the dust and H I-disk is observed for this range of H I deficiencies in other Virgo cluster galaxies (Cortese et al., 2010). The situation is different for M 99, which is not H I-deficient (H I-def= −0.1). Figure 1 clearly shows that the H I emission is much more extended than the submm at least to the north. Interestingly, this

---

[4] Image Reduction and Analysis Facility (IRAF)
http://iraf.noao.edu/

extended H I halo (Chung et al., 2009) however might be barely detected, but at the moment we cannot exclude that this is caused by residual background inhomogeneities coupled with a cluster of unresolved background sources. We can however exclude the presence of submm emission corresponding to the giant H I tail of M 99 (Haynes et al., 2007) to the southwest and we also find no measured flux associated with the extended low surface brightness feature to the southwest of M 100 (Chung et al., 2009).

The left column in Figure 2 shows the radial profiles obtained by the ellipse fitting to the smoothed maps. The MIPS and H I profiles agree with the published ones by Muñoz-Mateos et al. (2009b) and Chung et al. (2009), respectively. For M 99, the MIPS and SPIRE profiles follow similar trends including a weak radial break in the profile, i.e., a change in the slope, at $\approx 0.6 \times R25$, and a broken exponential is a more accurate fit than a single exponential (e.g. Pohlen & Trujillo, 2006, for more background on breaks). This break is also visible in the optical profile shown by Muñoz-Mateos et al. (2009b). The same is true for M 100, which also exhibits a more obvious break at around the same distance (it is even more striking in the profile at native resolution presented by Sauvage et al., 2010). This is the first time we see these breaks clearly in the dust distribution, while they are well-known at optical wavelengths. None of the so far presented hypotheses for the origin of these breaks have addressed this before (see e.g. the recent review by Vlajić, 2010, for references) and it will be another pice of the puzzle to be explained by the various proposed models. The rising profile in the inner part of M 100 is related to the more prominent bulge, bar, or inner-disk component, which is discussed in more detail in Sauvage et al. (2010).

To investigate the variation in submm colours as a function of radius we plot in the middle column of Figure 2 the ratio of the SPIRE bands $f350/f500$ to $f250/f350$. These are colour temperature indices. The advantage of using these instead of a derived dust mass is that they are independent of the specific, not yet well studied, model assumptions in this new wavelength range. They both decrease with radius, which suggests that the dust in the outermost regions is colder than in the centre of the galaxies. This is naturally explained by an interstellar radiation field becoming less intense in the outskirts. Our profiles are very similar to those of M 81 presented in Bendo et al. (2010b), who argue that the radial variation is driven by heating from the evolved stars in the galaxy. The observed range of flux ratios along the galactic radii is the same as found for a sample of galaxies with a wide variety of morphologies using integrated SPIRE fluxes (Boselli et al., 2010b). Interestingly, the agreement between their integrated and our resolved analysis extends beyond the colour profiles as shown in the right panels of Fig. 2, where we couple our colour gradients to the metallicity gradient published by Skillman et al. (1996) renormalised to the [OIII]/[NII] base of Pettini & Pagel (2004). The trend we observe radially for M 99 and M 100 matches the fit to the integrated properties of the Boselli et al. (2010b) sample very well. Both $f350/f500$ and $f70/f160$ (albeit only very weakly) decrease with the radially decreasing metallicity. This is again expected since a lower activity of star formation in the outer parts, as observed by Wilson et al. (2009), consequently entails lower metallicities.

In Fig. 3 we finally show the ratio of the total gas mass (H I plus H$_2$)[5] to 500μm flux ratio for the two galaxies. Since the 500μm flux is a proxy of the dust mass, this provides a "model-

---

[5] We use a radially constant X-factor as given in Kuno et al. (2007)
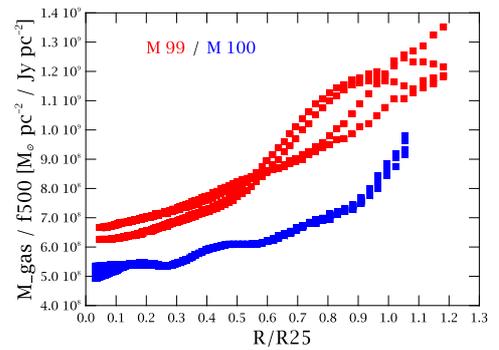
Fig. 3. Total gas mass (H I plus H$_2$) to SPIRE 500μm flux ratio.

independent" indication of the radial evolution of the dust-to-gas ratio. There is a clear trend visible with the gas-to-dust ratio increasing radially, which is consistent with earlier results (Muñoz-Mateos et al., 2009a; Bendo et al., 2010a), but the exact shape needs to be revised once a proper SED dust modelling including the new SPIRE bands is available.

In conclusion, we have found that the dust emission can be traced by the SPIRE bands at least out to the optical radius and beyond. The dust shows the same breaks in the radial profile as seen in the optical. The H I is only slightly more extended but this needs to be regarded here in the context of the cluster environment. The SPIRE colour temperature indices decrease with radius following the measured trends in metallicity, and the extent of the measured values along the galaxies' radii is consistent with the integrated properties of galaxies with a variety of morphologies. We have shown evidence of a radially rising gas-to-dust ratio. These results provide the first indication of the improved capabilities *Herschel* can offer for studying the resolved dust distribution in galaxies.

References

Bendo, G. J., Wilson, C. D., Warren, B. E., et al. 2010a, MNRAS, 402, 1409
Bendo, G., et al. 2010b, this volume
Boselli, A., et al. 2010a, PASP, 122, 261
Boselli, A., et al. 2010b, this volume
Boselli, A., & Gavazzi, G. 2006, PASP, 118, 517
Calzetti, D. 2001, PASP, 113, 1449
Cayatte, V., Kotanyi, C., Balkowski, C., & van Gorkom, J. H. 1994, AJ, 107, 1003
Chung, A., van Gorkom, J. H., Kenney, J. D. P., Crowl, H., & Vollmer, B. 2009, AJ, 138, 1741
Cortese, L., Davies, J. I., Pohlen, M. et al. 2010, this volume
de Vaucouleurs, G., de Vaucouleurs, A., Corwin, H.G., Buta, R.J., Paturel, G., & Fouque, J.B. 1991, Third reference catalogue of bright galaxies, Springer-Verlag New York
Draine, B. T. 2003, ARA&A, 41, 241
Gordon, K. D., Rieke, G. H., Engelbracht, C. W., et al. 2005, PASP, 117, 503
Griffin, M., et al. 2008, Proc. SPIE, 7010, 80
Griffin, M., 2009, SPIRE Technical Note, SPIRE-UCF-DOC-002890, Issue 7, 12 May 2009
Griffin, M., et al. 2010, this volume
Haynes, M. P., Giovanelli, R., & Kent, B. R. 2007, ApJ, 665, L19
Haynes, M. P., & Giovanelli, R. 1984, AJ, 89, 758

Kennicutt, R. C., Jr., Armus, L., Bendo, G. J., et al. 2003, PASP, 115, 928

Kuno, N., et al. 2007, PASJ, 59, 117

Mei, S., et al. 2007, ApJ, 655, 144

Muñoz-Mateos, J. C., et al. 2009**a**, ApJ, 701, 1965

Muñoz-Mateos, J. C., et al. 2009**b**, ApJ, 703, 1569

Ott, S. 2010, in ASP Conference Series, Astronomical Data Analysis Software and Systems XIX, Y. Mizumoto, K.-I. Morita, and M. Ohishi, eds., in press

Pettini, M., & Pagel, B. E. J. 2004, MNRAS, 348, L59

Pilbratt et al. 2010, this volume

Pohlen, M., & Trujillo, I. 2006, A&A, 454, 759

Sauvage, M., et al. 2010, this volume

Skillman, E. D., Kennicutt, R. C., Jr., Shields, G. A., & Zaritsky, D. 1996, ApJ, 462, 147

Swinyard, B. M., Ade, P. A. R., Baluteau, J.-P., et al. 2010, this volume

Vlajić, M. 2010, PASA in press, arXiv:1003.2565

Wilson, C. D., et al. 2009, ApJ, 693, 1736

[1] School of Physics and Astronomy, Cardiff University, Queens Buildings The Parade, Cardiff CF24 3AA, UK

[2] Astrophysics Group, Imperial College, Blackett Laboratory, Prince Consort Road, London SW7 2AZ, UK

[3] Laboratoire d'Astrophysique de Marseille, UMR6110 CNRS, 38 rue F. Joliot-Curie, F-13388 Marseille France

[4] Sterrenkundig Observatorium, Universiteit Gent, Krijgslaan 281 S9, B-9000 Gent, Belgium

[5] Jet Propulsion Laboratory, Pasadena, CA 91109, United States; Department of Astronomy, California Institute of Technology, Pasadena, CA 91125, USA

[6] Instituto de Astrofísica de Canarias, vía Láctea S/N, E-38200 La Laguna, Spain

[7] CEA, Laboratoire AIM, Irfu/SAp, Orme des Merisiers, F-91191 Gif-sur-Yvette, France

[8] Institut d'Astrophysique de Paris, UMR7095 CNRS, Université Pierre & Marie Curie, 98 bis Boulevard Arago, F-75014 Paris, France

[9] Department of Physics & Astronomy, University of California, Irvine, CA 92697, USA

[10] Observational Cosmology Lab, Code 665, NASA Goddard Space Flight Center Greenbelt, MD 20771, USA

[11] Department of Astrophysical and Planetary Sciences, CASA CB-389, University of Colorado, Boulder, CO 80309, USA

[12] ESA Astrophysics Missions Division, ESTEC, PO Box 299, 2200 AG Noordwijk, The Netherlands

[13] Astronomy Centre, Department of Physics and Astronomy, University of Sussex, UK

[14] Mullard Space Science Laboratory, University College London, Holmbury St Mary, Dorking, Surrey RH5 6NT, UK

[15] Dept. of Physics & Astronomy, McMaster University, Hamilton, Ontario, L8S 4M1, Canada

[16] School of Physics & Astronomy, University of Nottingham, University Park, Nottingham NG7 2RD, UK

[17] Istituto di Fisica dello Spazio Interplanetario, INAF, Via del Fosso del Cavaliere 100, I-00133 Roma, Italy

[18] Infrared Processing and Analysis Center, California Institute of Technology, Mail Code 100-22, 770 South Wilson Av, Pasadena, CA 91125, USA

[19] Centre for Astrophysics Research, Science and Technology Research Centre, University of Hertfordshire, College Lane, Herts AL10 9AB, UK

[20] University of Padova, Department of Astronomy, Vicolo Osservatorio 3, I-35122 Padova, Italy

[21] Observatoire Astronomique de Strasbourg, UMR 7550 Université de Strasbourg - CNRS, 11, rue de l'Université, F-67000 Strasbourg

[22] UK Astronomy Technology Center, Royal Observatory Edinburgh, Edinburgh, EH9 3HJ, UK

[23] Institut für Astronomie, Universität Wien, Türkenschanzstr. 17, A-1180 Wien, Austria